Applied Surface Science 60/61 (1992) 498–504
North-Holland

applied
surface science

Interfacial X-ray oscillations during growth of Pd_2Si on Si(111)

I.K. Robinson, P.J. Eng
AT&T Bell Laboratories, Murray Hill, NJ 07974, USA

P.A. Bennett and B. DeVries
Physics Department, Arizona State University, Tempe, AZ 85287, USA

Received 20 November 1991; accepted for publication 3 December 1991

Measurements were made by X-ray diffraction of the in-situ growth of Pd_2Si films on Si(111) at room temperature. Initially the growth is commensurate with lattice matching between the film and substrate, giving rise to a strained film. Above a critical thickness, the film relaxes to an unstrained state, but retains its epitaxial relationship. During both phases of growth, intensity oscillations are seen that correspond to the formation of an interfacial layer.

1. Introduction

Oscillation of a diffraction signal is a widely used indicator of layer-by-layer growth during molecular beam epitaxy (MBE) [1]. Usually this refers to the signal in a reflection high energy electron diffraction (RHEED) experiment, but oscillation can also be seen in low energy electron diffraction (LEED) [2] or X-ray diffraction [3]. This intensity oscillation corresponds to the alternation of completely and fractionally occupied layers of atoms during the growth. The frequency of oscillation is the growth rate in layers per second. The amplitude tends to decay in time because different parts of the growing sample become out of phase with each other. The oscillations are then restored when the growth is stopped and restarted after allowing the surface to anneal to the flat starting state once again. Sometimes several hundred oscillations can be observed.

Pd_2Si is known to form spontaneously at room temperature by reaction of a deposit of Pd on a Si(111) surface [4–7], and has been studied by a variety of techniques. Rutherford backscattering spectroscopy (RBS) [4] has shown that the silicide formation taken place at room temperature giving the Pd_2Si stoichiometry, at least between 2 and 10 monolayers (ML). Auger electron spectroscopy (AES) and electron energy loss spectroscopy (EELS) [5] have shown variations in chemical state up to 3 ML. LEED has found evidence for $\sqrt{3} \times \sqrt{3}$ and 3×3 structures, again for coverages greater than 3 ML [6]. RHEED has also seen a $\sqrt{3} \times \sqrt{3}$ structure that is simply related to the bulk Pd_2Si phase [7].

2. X-ray diffraction method

X-ray diffraction, particularly when enhanced by the use of synchrotron radiation, has been applied to the study of surfaces over the past 10 years [8,9]. More recently advantage has been taken of the penetrating property of X-rays to extend the technique to buried interfaces [10]. Depending on the angle of incidence and on the material, the typical range of penetration is from 10 to 10000 Å, so is well-matched to the study of thin films as well as interfaces in thin-film systems. The monolayer sensitivity comes firstly from from having sufficient flux to see a signal, and secondly from the special symmetry of the

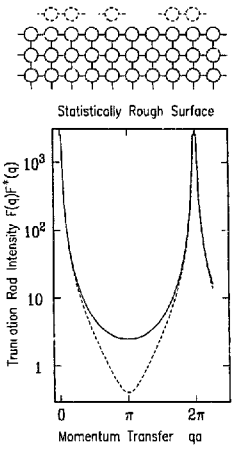

Fig. 1. Idealized model of a surface with a partial layer of extra atoms. Below is the calculated diffraction intensity given by eqs. (2) and (3), as a function of the momentum transfer along the direction perpendicular to the surface.

diffraction being studied. This second point arises because of the existence of crystal truncation rods (CTRs), discovered in 1986 [11]. Because the understanding of CTRs is central to the discussion of our results the relevant theory will now be elaborated.

The bold lined part of the picture at the top of fig. 1 shows an ideally terminated simple cubic lattice of atoms, representing a surface. The diffraction from this object can be represented as a sum over layers at positions z_j,

$$F(q) = f(q) \sum_{j=0}^{\infty} \rho_j \, e^{iqz_j}, \qquad (1)$$

where q is the momentum transfer and $f(q)$ is the atomic form factor. The set of layer densities (occupancies) ρ_j are unity in this simple case. For the undistorted lattice with layers of uniform spacing a,

$$F(q) = f(q) \frac{1}{1 - e^{iqa}}. \qquad (2)$$

The modulus squared of eq. (2) is the solid curve plotted in fig. 1. The intensity diverges every 2π where the bulk Bragg peaks lie because we have not included any of the attenuation due to absorption. In between there is the characteristic intensity distribution of the CTR, which, as we show below, is surface sensitive. These diffraction features are *rod-like* because they are diffuse in the direction shown, but sharp in cross section, when the momentum transfer is varied parallel to the surface.

We now consider the case of a partially occupied layer present as indicated by the dashed atoms in fig. 1. We assume the atoms to be randomly distributed on lattice sites, without bunching into islands or separation by repulsion that would give rise to lateral correlations, at least on the length scale of the instrumental coherence. This is what we mean by a *statistically rough* surface. We let the partial occupancy be ρ_0, with $\rho_j = 1$ for $j = 1$ to ∞. The evaluation of eq. (1) now gives,

$$F(q) = f(q) \left[\rho_0 + \frac{e^{iqa}}{1 - e^{iqa}} \right]. \qquad (3)$$

This is plotted as the dashed curve in fig. 1 with $\rho_0 = 0.6$. It is clear that there are big changes at the center of the reciprocal space zone due to the extra atoms. As we get further and further from the Bragg peaks we become more and more surface sensitive. Exactly the same is true of the terminated lattice and the extra atoms are at an interface: the breaking of the crystal's translational symmetry creates a rod of diffraction along the perpendicular to the cutting plane. In an experiment, we can identify such features by their rod-like symmetry and intensity distribution alone. All diffraction from the bulk crystal is concentrated in the intensity divergences (Bragg peaks) in fig. 1; all diffraction from point and line defects can be filtered out as background. Thus we are able to use spatial filtering to separate only

the rod-like features from all other diffraction, and thus isolate the 2D interfaces in the problem.

It is now obvious that in the case of a growing interface where the layers gradually fill in and become complete before the next one starts (layer-by-layer growth), the interface will alternate between the solid and dashed state in fig. 1. The diffraction will alternate between the solid and dashed curves also. If we measure near the midpoint of the CTR, we therefore can expect to see dramatic intensity oscillations.

3. Experimental procedures

Diffraction measurements were made on beamline X16A at the National Synchrotron Light Source (NSLS) in Brookhaven, USA. This is a dedicated surface X-ray diffraction facility with on-line surface/thin-film preparation and in-situ characterization. The motions of a precision X-ray diffractometer are passed through the vacuum wall, while the incoming and outgoing beams use a wide X-ray window made of Be [12]. To control the orientation of the optical surface separately from the crystallographic setting, we used five diffractometer angles in a 5-circle calculation [13].

The incident beam was focused with a toroidal Pt-coated mirror and monochromated by two parallel Si(111) crystals to give narrow energy bandwidth and small divergence. The wavelength was 1.611 Å corresponding to an energy of 7.695 keV. The diffracted beam was collimated with two 2 mm slits 0.5 m apart in the diffraction plane and detected with a position-sensitive detector (PSD) oriented perpendicular to the plane. The counts received were binned into 5 slices 2 mm wide and recorded simultaneously at each measurement setting.

The hexagonal convention was chosen for the substrate crystallographic unit cell, as shown in fig. 2. This maintains a pure index L for the out-of-plane direction. Indices h and k span the in-plane directions. Fig. 3 shows the corresponding reciprocal lattice and a typical h-scan that will be referred to later. The substrate bulk Bragg peaks 113, 111, 220 and $11\bar{1}$ therefore index as 105, 003, 104 and 101 as shown and are connected by the CTRs. With this choice of unit cell, the bin separation of the PSD is 0.05 units of c^*.

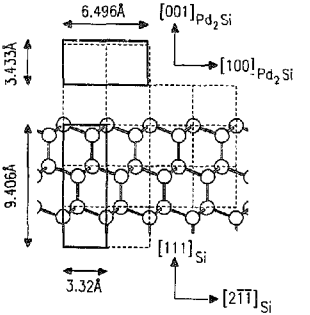

Fig. 2. Projected side view along $[01\bar{1}]_{Si}$ of a Si lattice ending with a (111) surface. The hexagonal unit cell used for indexing the lattice is the thick vertical box superimposed. This box is oblique by 30° to the plane of the page, so appears foreshortened by $\sqrt{3}/2$. The horizontal box drawn floating above the surface is the ac plane of the hexagonal unit cell of Pd_2Si drawn to scale. Notice the close lattice match to a $\sqrt{3} \times \sqrt{3}$ supercell of the substrate.

The Si(111) substrates were cleaned by light sputtering and annealing to 1500 K, as measured with an optical pyrometer. The first cleaning

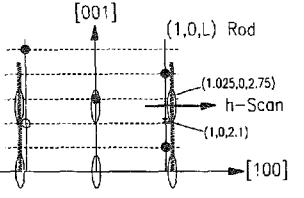

Fig. 3. Reciprocal lattice corresponding to fig. 2. The filled circles are the substrate bulk Bragg peaks 113, 111, 220 and $11\bar{1}$, respectively, from top-left to bottom-right. The open circles is the diamond-forbidden 002. Vertical lines are substrate CTRs indexed (-1, 0, L), (0, 0, L) and (1, 0, L). Vertical shaded lines are CTRs from the relaxed film with its principal Bragg peaks, such as (1.025, 0, 2.75) marked as ellipses.

round on a fresh wafer produced a 7×7 reconstruction; subsequent rounds only gave 1×1's, presumably because of residual metal contamination. Pd was deposited from a hot wire at a rate of ~ 0.02 Å/s. The accumulated deposit thickness was recorded with a quartz balance, calibrated for geometric factors assuming the evaporation was isotropic, but these were somewhat inaccurate. There was a resulting $\sim 10\%$ reproducibility from run to run partly because it was coupled to the sample orientation on the goniometer. In addition there was a $\sim 50\%$ uncertainty in overall thickness calibration, pending future calibration of standard samples by Rutherford backscattering spectroscopy. The thickness monitor also suffered from a thermally induced drift when the Pd wire was heated, which added to the uncertainty. All thicknesses quoted in this paper are those for bulk Pd metal, assuming bulk density of 12.16 g/cm^3. Pd_2Si (9.69 g/cm^3) thicknesses will be 1.42 times bigger.

4. Results

We conducted a wide exploration of possible structures at a number of different coverages to obtain an overview of the general behavior of the Pd/Si(111) system at room temperature. We found qualitatively different results above and below a threshold value of ~ 18 Å Pd coverage, in agreement with earlier work [4,5]. Below 18 Å Pd coverage, all diffraction features were localized along the substrate CTRs, such as the $(1, 0, L)$ rod labelled in fig. 3. Above 18 Å Pd coverage, new peaks appeared at the incommensurate rod positions shaded in fig. 3.

This high-coverage phase was straightforward to identify. The intensity along the (shaded) $(1.025, 0, L)$ rod was featureless except for strong peaks at $L = 0$ and $L = 2.75$. The $(-1.025, 0, L)$ rod was essentially the same, suggesting a phase with hexagonal symmetry, not cubic as in the bulk substrate. The derived lattice parameters, $a = 6.489$ Å and $c = 3.42$ Å, assuming the $\sqrt{3} \times \sqrt{3}$ larger unit cell, agree within error of those for bulk Pd_2Si, namely $a = 6.496$ Å and $c = 3.433$ Å [14]. We conclude that the film above 18 Å Pd coverage is epitaxial, but incommensurate, Pd_2Si with the epitaxial relationship shown in fig. 2, $(001)_{Pd_2Si} \| (111)_{Si}$ and $[100]_{Pd_2Si} \| [2\bar{1}\bar{1}]_{Si}$.

The low-coverage phase is harder to identify because the diffraction from the film interferes with the CTRs of the substrate. However, scans along both the $(1, 0, L)$ and $(-1, 0, L)$ rods showed, in addition to the substrate peaks shown, new broad peaks at $L = 0$ and $L \approx 3$. We conclude that the film below 18 Å Pd coverage is epitaxial and commensurate Pd_2Si with the same epitaxial relationship. The film is considerably strained, with a 2.5% expansion in both in-plane directions and a $\sim 10\%$ contraction out-of-plane. Because the film is so thin and because the out-of-plane peak was at our instrument's angle limit, we could not establish its c parameter any better than this.

To probe the dynamics of the film formation we measured some of the characteristic diffraction features as a function of coverage θ during in-situ deposition. Panel (a) of fig. 4 shows the intensity at $(1, 0, 2.1)$ which sees both the film and the substrate CTR on its descent from the Bragg peak at 101. The substrate alone gives the intensity value at $\theta = 0$. For $\theta > 0$ this interferes with the amplitude from the arriving Pd that is forming the initial commensurate Pd_2Si phase. Dramatic oscillations of the intensity are seen here as θ increases. The period starts at 6.9 Å but shortens after the first three oscillations to 5.4 Å for the rest of the run.

Panel (b) of fig. 4 shows the intensity at $(1.02, 0, 2.75)$ which measures the total amount of incommensurate Pd_2Si formed. The abrupt rise at ~ 18 Å clearly illustrates the point made above that the incommensurate phase appears only after a delay. Since we found no evidence for a change of structure between the two phases, other than the presence or absence of strain, we claim this to be an example of a *critical thickness* phenomenon. In other words, initial growth produces strained hexagonal Pd_2Si up to the critical thickness of 18 Å Pd (which is 26 Å of film, or 6 unit cells). Above the critical thickness, the film switches to its relaxed incommensurate state, which is retained for all subsequent growth.

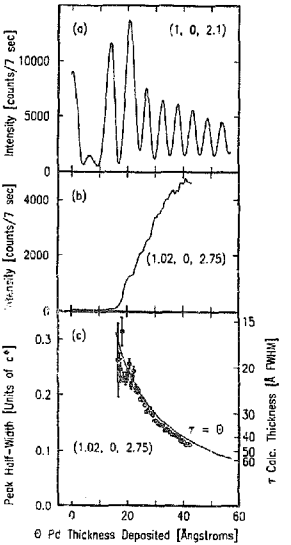

Fig. 4. (a, b) Intensity measured at single reciprocal space points as a function of Pd coverage. The two points, indicated in fig. 3, are sensitive to the commensurate low-coverage and incommensurate high-coverage phases of Pd_2Si, respectively. (c) Half-width along the L-direction of the incommensurate peak measured simultaneously with (b). The curve is calculated using eq. (4).

Critical thickness is simply understood from energetic considerations [15]. Since the excess free energy per unit area due to strain, $A\tau$, is proportional to film thickness, τ, and the interfacial energy per unit area due to misfit of an incommensurate film, B, is not, the choice of lowest energy state will necessarily depend on whether τ is less than or greater than $\tau_c = B/A$.

During the uptake, we could obtain the evolution of the width of the diffraction peak along the rod L-direction by observing the distribution along the PSD. For the position (1.02, 0, 2.75), a clear peak was seen. A Gaussian distribution fitted quite well. The Gaussian half-width is plotted as a function of deposit thickness in fig. 4c. This half-width ΔL is inversely related to the thickness τ of the film by the Fourier transform relation,

$$\tau[\mathrm{FWHM}] = \frac{4\sqrt{\ln 2}}{\Delta L[1/\sigma]c^*}. \qquad (4)$$

The width is thus mapped onto a film thickness scale on the right-hand side of the figure, and the solid line that passes roughly through the data is the curve $\tau = \theta$ that would correspond to a film thickness with the density of Pd. Considering that the density of Pd in Pd_2Si is smaller, the film should be correspondingly thicker, however. We see immediately that the thickness is proportional

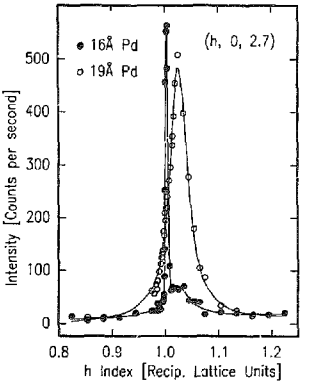

Fig. 5. Scans along the h reciprocal lattice direction parallel to the interface, as indicated in fig. 3. The two Pd thicknesses shown are slightly below and slightly above the critical thickness. The data were taken by interrupting the deposition: the actual thicknesses seen with the quartz balance were somewhat lower and have been adjusted for consistency with the horizontal scale of fig. 4.

to coverage. The density scale-factor is within the uncertainty of our coverage determination.

Lastly, fig. 5 shows the critical thickness transition in the form of h-scans through the two rods along the trajectory indicated in fig. 3. The lower coverage curve has a sharp peak at the CTR position $h = 1$ and a slight hint of a incommensurate peak. The second curve with 20% more Pd deposit shows no CTR peak at all and a large, broad peak at $h = 1.025$. The fit curves passing through the data are a Gaussian of half-width $\Delta h = 0.002$ for the CTR peak and a Lorentzian of half-width $\Delta h = 0.02$ for the incommensurate Pd_2Si peak. The former is resolution-limited and indicates very-long-range lateral order, while the latter suggests a relatively incoherent phase with a typical grain size of 100 Å parallel to the interface. The incommensurate phase is, however, epitaxial. The half-width of the peak in the transverse direction was $\Delta k = 0.03$, also with a Lorentzian distribution. This indicates either a finite lateral grain size of ~ 70 Å (parallel to the interface) or a mosaic spread of 3.5° (FWHM) or else a combination of both.

5. Discussion

We believe we understand the behavior above the critical thickness transition for $\theta > \theta_c = 18$ Å Pd coverage: the peak positions align exactly with those published for bulk Pd_2Si [14], and the evolution of the peak width (fig. 4c) follows that expected for the amount of Pd deposited. Somewhat less clear is the evolution of the intensity of this phase in fig. 4b. We would expect a jump at $\theta_c = 18$ Å followed by a quadratic rise in peak intensity as the peak narrows. Instead we see an intensity that extrapolates approximately linearly to $\theta_c = 18$ Å, as if some of the deposited Pd were invisible. However, fig. 5 does show signs of coexistence of both the commensurate and incommensurate phases already at $\theta = 16$ Å. A likely explanation is that the critical thickness transition is simply broadened by inhomogeneities, that convert the expected intensity jump into a broad shoulder in fig. 4b.

A significant finding is that the CTR intensity continues to oscillate during this phase of growth, as seen in fig. 4a. While the deposited Pd appears to end up in the incommensurate phase, its route there clearly involves the substrate. The simplest mechanism that is consistent with our data is that Si is consumed in a layerwise manner at the $Pd_2Si/Si(111)$ interface. When a layer is partially consumed, we have the situation of the dashed curve in fig. 1 with a reduced CTR intensity; when the layer is used up, we return to the solid curve. The period of oscillation during $\theta > \theta_c$ is 5.4 Å of Pd, which implies 2.3 Si layers are consumed per period, assuming Pd_2Si stoichiometry. This period is within our thickness calibration error of 2 Si layers, and is not surprising because of the bilayer nature of the Si(111) surface (fig. 2). Assuming this model, we reach the satisfying conclusion that Si is used up in double layers and that this is the origin of the intensity oscillation for $\theta > \theta_c$. Of course we cannot rule out more complex mechanisms involving incorporation of the arriving Pd at the interface in a commensurate holding state before transfer to the incommensurate Pd_2Si.

The reaction between arriving Pd and Si clearly involves the $Pd_2Si/Si(111)$ interface, but it need not necessarily *take place* there. Two possible scenarios are that Si diffuses through the Pd_2Si phase to the surface to react with arriving Pd, or that Pd diffuses to the interface. The LEED pattern was diffuse throughout the deposition, indicating no ordered structures at the surface. Although surface models could still be constructed without the need for order, this result favors the model of an interface reaction.

The behavior below the critical thickness transition with $\theta < \theta_c = 18$ Å Pd coverage is not so well understood, because all diffraction is concentrated along a single CTR line and cannot be interpreted uniquely. As stated above, we believe the film to be in a strained Pd_2Si state that possesses the same structure as the relaxed state that forms later. Somehow the interference of the diffraction of such a film with the substrate gives a longer period of 6.9 Å and the wide variation of oscillation amplitudes in fig. 4a. There may be a sequence of intermediate structures involved. This

work is still in progress and will be published at a later time.

Acknowledgements

We have enjoyed discussions of this work with D. Eaglesham. NSLS is supported by the DOE under DE-AC02-76CH00016. P.A.B. and B.d.V. benefitted from a DOE Faculty and Student award. Partial support also came from NSF DMR8921124.

References

[1] J.H. Neave, B.A. Joyce, P.J. Dobson and N. Norton, Appl. Phys. A 31 (1983) 1.
[2] K.D. Gronwald and M. Henzler, Surf. Sci. 117 (1982) 180.
[3] E. Vlieg, A.W. Denier van der Gon, J.F. van der Veen, J.E. Macdonald and C. Norris, Phys. Rev. Lett. 61 (1988) 2241.
[4] R.M. Tromp, E.J. van Loenen, M. Iwami, R.G. Smeenk, F.W. Saris, F. Nava and G. Ottaviani, Surf. Sci. 124 (1983) 1.
[5] S. Nishigaki, T. Komatsu, M. Arimoto and M. Sugihara, Surf. Sci. 167 (1986) 27.
[6] J.G. Clabes, Surf. Sci. 145 (1984) 87.
[7] A. Oustry, J. Berty, M. Caumont, M.J. David and A. Escaut, Thin Solid Films 97 (1982) 295.
[8] I.K. Robinson, in: Handbook on Synchrotron Radiation, Vol. 3, Eds. D.E. Moncton and G.S. Brown (North-Holland, Amsterdam, 1991) p. 221.
[9] R. Feidenhans'l, Surf. Sci. Rep. 10 (1989) 105.
[10] I.K. Robinson, Mater. Res. Soc. Bull. 15 (1990) 38.
[11] I.K. Robinson, Phys. Rev. B 33 (1986) 3830.
[12] P.H. Fuoss and I.K. Robinson, Nucl. Instr. Meth. 222 (1984) 171.
[13] E. Vlieg, A.W. Denier van der Gon, J.F. van der Veen, J.E. Macdonald and C. Norris, Surf. Sci. 210 (1989) 301.
[14] K. Anderko and K. Schubert, Z. Metallkd. 44 (1953) 307.
[15] A.T. Fiory, J.C. Bean, L.C. Feldman and I.K. Robinson, J. Appl. Phys. 56 (1984) 1227.